Reaction Chemistry & Engineering

ROYAL SOCIETY OF CHEMISTRY

PAPER

View Article Online
View Journal | View Issue

Cite this: *React. Chem. Eng.*, 2023, **8**, 1719

Efficient and continuous furfural hydrogenation to furfuryl alcohol in a micropacked bed reactor†

Lian Duan,[a] Mengmeng Huang,[b] Zipin Peng,[b] Le Sang *[a] and Jisong Zhang *[b]

Received 18th February 2023,
Accepted 27th March 2023

DOI: 10.1039/d3re00098b

rsc.li/reaction-engineering

In this work, continuous furfural hydrogenation to furfuryl alcohol in micropacked bed reactors (μPBRs) is investigated. The performances of Cu-, Ni-, Pd-, and Pt-based catalysts for the furfural hydrogenation reaction are evaluated at different temperatures. Then the effects of solvent, pressure, gas and liquid flow rates, and initial concentration of furfural on the conversion of furfural and the yield of furfuryl alcohol are discussed. 100% furfuryl alcohol can be obtained under mild reaction conditions (80 °C and 0.6 MPa) with a reaction time of 65 s. For the catalytic transfer hydrogenation of FUR, μPBRs also provide excellent reaction performance (yield of furfural alcohol = 94.3%) with a reaction time of 194 s at 100 °C and 0.6 MPa. The space time yield of μPBRs is 0.51 kg L^{-1} h^{-1}, which is 1–2 orders of magnitude higher than those of conventional stirred tank reactors and packed bed reactors. Furthermore, the intrinsic reaction kinetics is established and the experimental data are also described by the Langmuir–Hinshelwood model. This work provides a more efficient, fast, continuous, and safe process for furfural hydrogenation reactions in μPBRs.

Introduction

The decrease of fossil resource reserves and excessive energy consumption are the major problems of mankind nowadays.[1] To overcome these issues, the development and efficient utilization of biomass energy can reduce fossil resource consumption and promote sustainable production of fuels and chemicals.[2] Furfural (FUR) is an important chemical intermediate that is commonly hydrogenated into a variety of highly valued chemicals (*e.g.* furfuryl alcohol (FA), tetrahydrofurfuryl alcohol (THFA), 2-methylfuran (2-MF), 2-methyltetrahydrofuran (2-THMF), *etc.*).[3] In this regard, about 65% of FUR is used to prepare FA with great industrial interest.[4] Up to now, FA is widely applied in the polymer industry (furan and phenolic resins), pharmaceutical intermediates (anti-ulcer drugs and vitamin C), and the synthesis of green solvents (THFA).[5]

FA can be generated by liquid-phase or gas-phase hydrogenation of FUR.[6] A larger number of metal catalysts have been designed to improve the selectivity of FUR hydrogenation and the yield of FA for the liquid-phase hydrogenation.[7–9] Precious metal catalysts such as Pd, Pt, and Ru have promising catalytic performances for the hydrogenation of FUR to FA. Salnikova *et al.*[10] studied Pd-containing catalysts stabilized by hypercrosslinked polystyrene for the hydrogenation of FUR in a stirred tank reactor (STR). The experimental results showed that the yield of FA was 48.6% with a reaction time of 3.5 h at 120 °C and 6 MPa. Taylor *et al.*[11] found that a Pt/γ-Al_2O_3 catalyst could selectively hydrogenate FUR to FA in a STR. The yield of FA was 79.2% with methanol solvent and a reaction time of 7 h at 50 °C and atmospheric pressure. Ramirez-Barria *et al.*[12] used 4 wt% Ru/graphene oxide catalysts to investigate selectively hydrogenation of FUR to FA in a batch reactor. The experimental results revealed that the FA yield was 91.4% for 5 h at 20 °C and 1 MPa. Although precious metal catalysts are effective for FUR hydrogenation, their industrial application is constrained by their large cost.[13]

For non-precious metal catalysts, Wang *et al.*[5] found that the yield of FA was 91% for 12 h at 180 °C and 3 MPa in a batch reactor with ferromagnetic Ni-doped lignin-derived ordered mesoporous carbon. Bimetallic Ni_3Fe_1/SiO_2 catalysts were reported to be favourable for the hydrogenation of FUR to FA.[14] Under the reaction conditions of 140 °C and 3.4 MPa, the yield of FA was 96.5% in a STR with 5 h reaction time. Gong *et al.*[7] prepared Cu/C–SO_3H catalysts for the selective hydrogenation of FUR to FA in STRs. The yield of FA was almost 100% at 105 °C and 0.4 MPa with a reaction time of 2 h. CuZnAl catalysts have also demonstrated remarkable catalytic performance with a FA yield of 99% for hydrogenation of FUR in STRs at 100 °C and 1 MPa, with 4 h

[a] *School of Chemistry and Chemical Engineering, Beijing Institute of Technology, Beijing 102488, P. R. China. E-mail: lesang@bit.edu.cn*
[b] *The State Key Lab of Chemical Engineering, Department of Chemical Engineering, Tsinghua University, Beijing 100084, P. R. China. E-mail: jiszhang@tsinghua.edu.cn*

† Electronic supplementary information (ESI) available. See DOI: https://doi.org/10.1039/d3re00098b

reaction time.[15] Catalytic transfer hydrogenation (CTH) is viewed as a promising path for the liquid phase hydrogenation reaction. Cu/C–SO_3H catalysts were demonstrated to prepare FA from FUR through CTH in a batch reactor.[7] The FA yield was 99.99% at 150 °C and 4 MPa N_2 with a reaction time of 5 h. Alumina also proved to be an effective catalyst for the hydrogenation of FUR to FA using secondary alcohols as solvents due to its active Lewis acid sites. The yield of FA was higher than 90% at 150 °C with 6 h reaction time in a batch reactor.[16] Yang *et al.*[17] prepared a novel oxygen-vacant Mn_3O_4 catalyst for CTH of FUR. A high FA yield (99%) was obtained at 220 °C with 4 h reaction time in isopropanol. Above all, Cu-based catalysts showed preferable selectivity for FA in STRs, but the batch operation and long reaction time restricted the industrial application for FUR hydrogenation to FA.

A continuous flow reactor is considered a continuous, efficient, and safe technology due to its small equipment size and better transport performance.[18] Continuous flow technology can precisely control the reaction process and time, which is advantageous in the conversion of biomass platform molecules into high value-added chemicals.[19] Wang *et al.*[20] used a Ni/C catalyst to compare the reaction performance of FUR hydrogenation between batch and continuous reactor modes. Based on the method of molecular hydrogenation, experimental results showed that 2-MF was generated (yield = 66%) in STRs at 200 °C and 3 MPa. FA (yield = 38%) and THFA (yield = 20%) could be produced in continuous flow reactors at 150 °C and 5 MPa. Garcia-Olmo *et al.*[21] investigated the selectivity and stability of FUR hydrogenation in an H-Cube mini flow reactor with a Ru/C catalyst. The results showed that the yield of FA was about 85% at 90 °C and 5 MPa within 34 s under the continuous flow process. However, high temperature (up to 230 °C) and high pressure (3–5 MPa) are still required for the hydrogenation of FUR to FA in continuous flow reactors. The continuous flow reactors for the FUR hydrogenation to FA multiphase process need to be further designed and optimized.

Recently, micropacked bed reactors (μPBRs), as a new type of continuous flow reactor, have been applied in biomass conversion processes, such as levulinic acid hydrogenation,[22] 5-hydroxymethylfurfural oxidation,[23] and dehydration of glucose[24] due to their excellent gas–liquid–solid mass transfer characteristics.[25,26] Meanwhile, μPBRs are characterized by easy catalyst immobilization and recovery as well as better heat transfer performance.[27–29] The intrinsic kinetics of the reaction can be determined quickly and accurately based on μPBRs.[30–32]

In this work, the efficient and continuous conversion of FUR to FA in μPBRs was investigated based on the methods of molecular hydrogenation and catalytic transfer hydrogenation. Firstly, the performances of Cu-, Ni-, Pd- and Pt-based catalysts for FUR hydrogenation were screened at different temperatures to obtain suitable catalysts in μPBRs. Then, the effects of solvent, pressure, hydrogen and FUR solution flow rates, and initial concentration of FUR on the conversion of FUR and the yield of FA were discussed. Finally, catalytic transfer hydrogenation of FUR to FA in μPBRs was also investigated. The performances of FUR hydrogenation in different reactors were compared and an intrinsic reaction kinetics model for the hydrogenation of FUR to FA was developed.

Experiments

Chemicals

Furfural with a purity of 99% was purchased from Shanghai Titan Co., Ltd. Furfuryl alcohol, 2-methylfuran, 2-methyltetrahydrofuran, and tetrahydrofurfuryl alcohol were purchased from Shanghai Macklin Biochemical Co., Ltd. The solvents methanol, ethanol, isopropanol, and 2-butanol were purchased from Shanghai Titan Co., Ltd., and the solvents ethyl acetate and toluene were obtained from Energy Chemical and Beijing Bailingwei Technology Co., Ltd, respectively. Pure hydrogen was supplied through a commercial hydrogen generator (Beijing Oushisheng Technology, Co., Ltd.). And nitrogen was obtained from Beijing Beiwen Gas Manufacturing Plant. Palladium/carbon (Pd/C, 3 wt%), platinum/carbon (Pt/C, 3 wt%), copper/silica (Cu/SiO_2, 20 wt%), and nickel/silica (Ni/SiO_2, 20 wt%) particle catalysts were purchased from Beijing Phaseflow Technology, Co., Ltd.

Catalyst characterization

The properties of the catalysts used in the experiments are shown in Table 1. The specific surface area, pore volume, and pore size of the catalysts were obtained by the Brunauer–Emmett–Teller (Autosorb-1-C, Quantachrome Instruments, USA) method after the samples were degassed under vacuum at 423 K for 6 h. It can be seen that the specific surface area of the carbon supports was significantly larger than that of the silica supports. As for the pore size, the silica supports were larger than the carbon supports.

Table 1 Properties of the catalysts used in this study

Catalyst	Particle size/μm	Surface area/$m^2\ g^{-1}$	Pore volume/$cm^3\ g^{-1}$	Pore size/nm
Cu/SiO_2	600	370.1	0.70	7.61
Ni/SiO_2	600	327.6	0.48	5.89
Pt/C	425	957.2	0.55	2.30
Pd/C	425	883.2	0.50	2.26

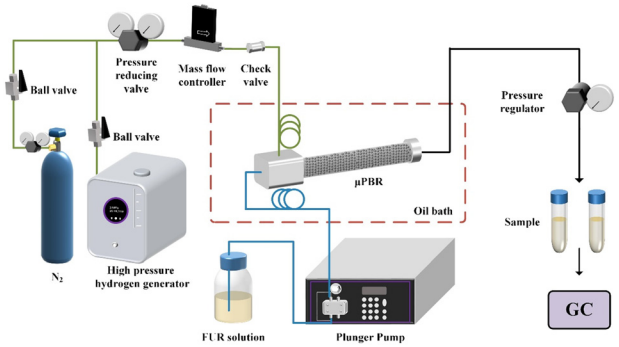

Fig. 1 Schematic overview of the experimental setup for the FUR hydrogenation study.

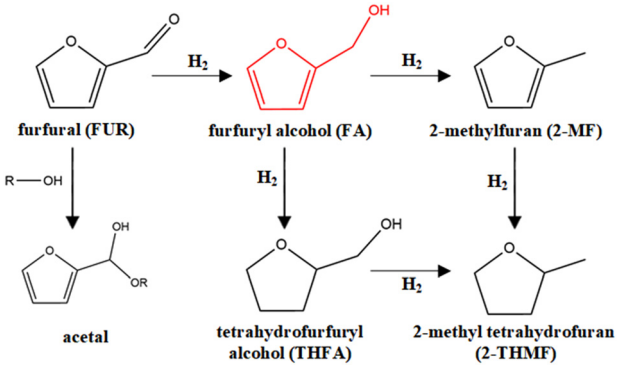

Fig. 2 Illustration of reaction pathways for FUR hydrogenation.

Equipment procedures for FUR hydrogenation

The schematic overview of the FUR hydrogenation reaction is shown in Fig.1. For the hydrogenation process, FUR solution in the liquid phase and hydrogen in the gas phase are delivered using a plunger pump (Beijing Oushisheng Technology, Co., Ltd.) and a gas mass flow controller (Beijing Sevenstar Electronics Co., Ltd.), respectively. For the CTH process, the gas is switched to nitrogen through the ball valve. After preheating by a coil, gas–liquid–solid or liquid–solid phases came into contact and reacted in a micropacked bed reactor with catalyst particles. For the process optimization section, reactors with a volume of 2.94 mL, an inner diameter of 3.87 mm, an outer diameter of 6.4 mm, and a length of 250 mm were applied. For the kinetic study section, the same volume (1.2 mL), with different inner diameters (3.87, 4.35, and 5.35 mm), and different reactor lengths (102, 79, and 53.5 mm) of the reactor were used. The temperature and pressure of the reaction were controlled by the oil bath and back pressure regulator, respectively. The outlet sample was collected every three times of the liquid residence time and then analyzed by gas chromatography (GC).

Analytical method

The product samples were analyzed by gas chromatography (Agilent, GC-8860) with an Agilent HP-5 column (30 m × 0.32 mm × 0.25 μm) and a FID. The temperature program was 30 °C for 3 min followed by heating to 45 °C for 1 min at a heating rate of 2 °C min^{-1} and increased to 280 °C at a heating rate of 30 °C min^{-1}. The typical GC signals of the reaction are shown in the ESI† (Fig. S1). The retention times of the reactants and products are as follows: 2-methylfuran (2-MF): 2.6 min, 2-methyltetrahydrofuran (2-THMF): 3.5 min, furfural (FUR): 8.9 min, furfuryl alcohol (FA): 10.4 min, tetrahydrofurfuryl alcohol (THFA): 11.7 min. Then, the conversion of FUR and the yield of the product can be obtained using eqn (1) and (2), respectively.

$$X = \frac{C_{FUR0} - C_{FUR}}{C_{FUR0}} \times 100\% \quad (1)$$

$$Y = \frac{C_{Product}}{C_{FUR0}} \times 100\% \quad (2)$$

where C_{FUR0} is the initial concentration of FUR, and C_{FUR} and $C_{Product}$ are the concentrations of FUR and the product, respectively.

Results and discussion

Performance evaluation of different catalysts

The product and reaction pathways for hydrogenation of FUR are depicted in Fig. 2. And the performance of various types of catalysts in the catalytic hydrogenation of FUR is shown in Fig. 3. From Fig. 3, it can be seen that the Cu/SiO_2 catalyst exhibited high catalytic activity with 100% conversion of FUR at a low temperature of 60 °C and 0.6 MPa. The highest yield of FA (99.6%) was obtained under mild reaction conditions of 80 °C and 0.6 MPa. With further increase of temperature,

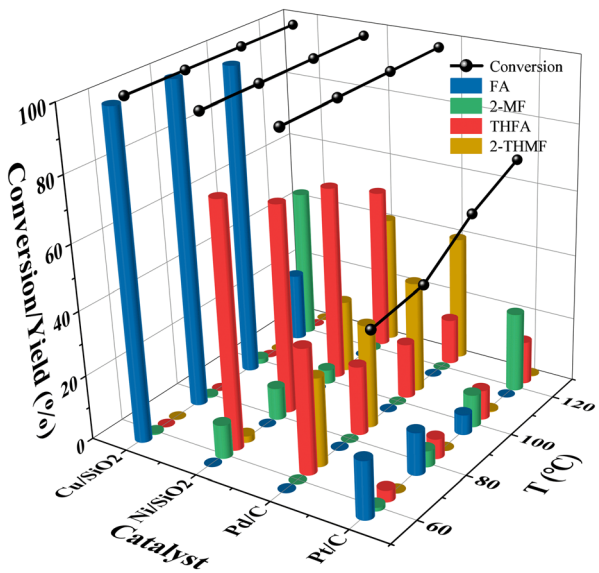

Fig. 3 Comparison of catalysts for FUR hydrogenation in μPBRs at different temperatures. Reaction conditions: 0.2 mol L^{-1} FUR in isopropanol, 0.6 MPa, 0.2 mL min^{-1}, 20 sccm.

the yield of FA decreased due to the excessive hydrogenation reaction of FA to produce 2-MF at high temperature. For the Ni/SiO_2 catalyst, the FUR hydrogenation product was mainly THFA (75.3% yield) at 60 °C. By reaction optimization, the THFA yield can reach up to 77.9% at 60 °C and 0.3 MPa as shown in the ESI† (Table S1). As the temperature increased, THFA was further converted to 2-THMF. The hydrogenation products of FUR in μPBRs with Ni/SiO_2 were significantly different compared to those with the Cu/SiO_2 catalyst. It is mainly ascribed that the Ni/SiO_2 catalyst exhibited great activity for aromatic furan ring hydrogenation.[33] For the noble metal catalyst Pd/C, the high catalytic activity resulted in 100% conversion of FUR in the range of 60–180 °C as depicted in Fig. 3 and the ESI† (Table S2). On the one hand, there was no FA production because the highly active metal Pd adsorbed the furan ring more easily, thus promoting the generation of THFA at low temperature.[34] On the other hand, the yield of 2-THMF can reach 67.8% as the temperature increases to 180 °C due to the eliminated C═O bonds.[35] For the Pt/C catalyst, the FUR hydrogenation activity is lower than that for Pd/C in μPBRs, especially at low temperatures (<100 °C) as shown in the ESI† (Table S2). This may be due to the strong affinity and sorption of H_2 on the Pd surface.[36] In summary, Cu/SiO_2 is preferred for the selective catalytic hydrogenation of FUR to FA in μPBRs. Also, Cu/SiO_2 can operate stably for 16 h as shown in the ESI† (Fig. S2) . Therefore, the performance of FUR hydrogenation in μPBRs was further investigated in μPBRs with Cu/SiO_2 catalysts at 80 °C.

Effect of solvents

The solvent affects the external mass transfer performance between the gas–liquid–solid phase, the solubility of hydrogen, and the adsorption mechanism of the solvent molecules on the active sites, leading to variations in the hydrogenation reaction performance.[26,28,33] Solvents for FUR hydrogenation are mainly divided into protonic solvents (*e.g.* methanol, ethanol, isopropanol, 2-butanol, *etc.*) and aprotic organic solvents (*e.g.* ethyl acetate and toluene).[20] The effects of solvents on the hydrogenation performance of FUR are shown in Table 2. For the protonic solvents, isopropanol gave the best FUR conversion performance (100%) and FA yield (99.5%). With respect to methanol and ethanol, the main product was acetal *via* the reaction between FUR and the alcohol solvent. It is attributed that the overly strong interaction of FUR with the alcohol solvent inhibits the hydrogenation process of FUR on the Cu catalyst.[37] For the aprotic organic solvents, the conversion of FUR in ethyl acetate was greater than that in toluene. This may be a result of the lower viscosity of ethyl acetate with low external mass transfer resistance.[26] It is worth noting that the selectivity to FA was 100% when ethyl acetate was used as the solvent under mild reaction conditions of 80 °C and 0.1 MPa. Ethyl acetate has been widely used for FUR hydrogenation reactions in continuous mode due to its high selectivity.[21,38] Therefore, isopropanol and ethyl acetate were used as solvents in subsequent experiments for the hydrogenation of FUR.

Effect of operating pressure

The operating pressure affects the solubility of hydrogen in the solvent, which in turn affects the reaction conversion and selectivity.[28] The effect of operating pressure on the conversion of FUR and the product yield can be shown in Fig. 4. From Fig. 4(a), it can be seen that for isopropanol as the solvent, the yield of FA slightly increased when the reaction pressure was increased to 0.6 MPa due to the decrease of by-product acetal. This phenomenon can be explained by the fact that the higher hydrogen pressure resulted in higher hydrogen concentration in FUR solution and reacted to inhibit the side reaction between FUR and isopropanol.[39] However, when the hydrogen pressure was further increased, some of the FA continues to undergo the hydrogenation reaction to produce 2-MF and other high boiling point by-products. As a result, the yield of FA decreased when the pressure was increased from 0.6 MPa to 3.1 MPa. In Fig. 4(b), with ethyl acetate as the solvent, the conversion of FUR reached 100% and the yield of FA was 99.3% when the pressure was raised from 0.1 to 0.6 MPa. The main reason could be that the hydrogenation of FUR is promoted by the increase in active hydrogen on the catalyst resulting from the higher hydrogen pressure. When the pressure was increased from 0.6 MPa to 3.1 MPa, the conversion of FUR was unchanged and the yield of FA was slightly decreased due to the generation of 2-MF. Considering the energy consumption, the optimal process conditions will be investigated at 0.1 MPa for isopropanol and 0.6 MPa pressure for ethyl acetate.

Table 2 Effect of solvents for FUR hydrogenation in μPBRs

Solvent	Conversion/%	FA yield/%	Acetal by-product yield/%
Methanol	67.5	0	67.5
Ethanol	57.6	0	57.6
Isopropanol	100	99.5	0.5
2-Butanol	47.9	26.9	21
Ethyl acetate	52.9	52.9	0
Toluene	38.4	38.0	0

Reaction conditions: 0.2 mol L^{-1} FUR, 80 °C, 0.1 MPa, 0.2 mL min^{-1}, 20 sccm.

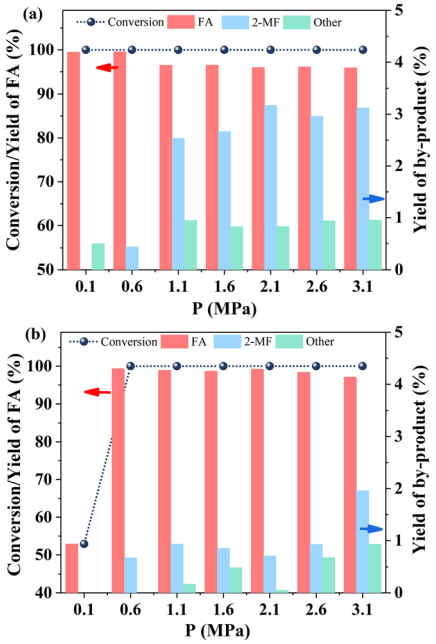

Fig. 4 Effect of operating pressure on the conversion and yield. Reaction conditions: 0.2 mol L^{-1} FUR, 80 °C, 0.2 mL min^{-1}, 20 sccm, (a) isopropanol and (b) ethyl acetate.

Effect of the gas flow rate

The gas flow rate of hydrogen affects the gas–liquid–solid mass transfer performance and mean residence time for the hydrogenation process in the microreactor.[40] As can be seen in Fig. 5(a) and (b), the increase in the gas flow rate leads to a decrease in the FA yield, in particular at a high gas flow rate. It is mainly attributed that an increase in the gas flow rate decreases the mean residence time, leading to the insufficient contact among the gas–liquid–solid catalysts. Based on the experimental results, a gas flow rate of 20 sccm was chosen as the optimized condition for the subsequent experiments.

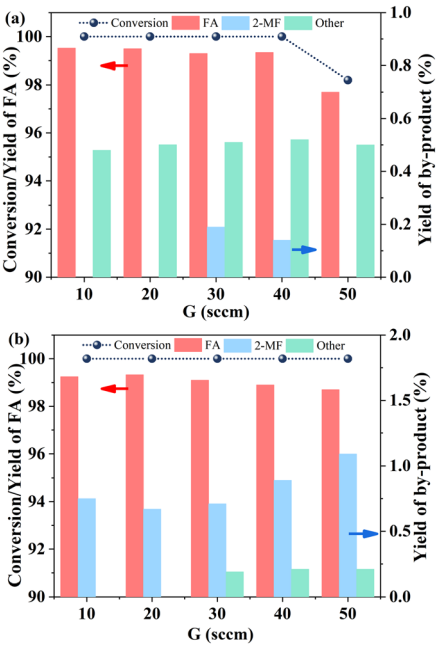

Fig. 5 Effect of the gas flow rate on the conversion and yield. Reaction conditions: 0.2 mol L^{-1} FUR, 80 °C, 0.2 mL min^{-1}, (a) isopropanol, 0.1 MPa and (b) ethyl acetate, 0.6 MPa.

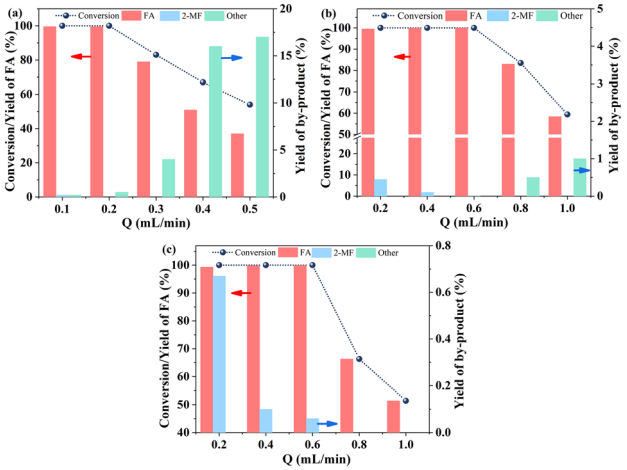

Fig. 6 Effect of the liquid flow rate on the conversion and yield. Reaction conditions: 0.2 mol L^{-1} FUR, 80 °C, 20 sccm, (a) isopropanol, 0.1 MPa, (b) isopropanol, 0.6 MPa, and (c) ethyl acetate, 0.6 MPa.

Effect of the liquid flow rate

The liquid flow rate affects the hydrodynamics and gas–liquid–solid interaction, and thus the hydrogenation performance of the reactor.[41] The effect of the liquid flow rate on the hydrogenation performance of FUR is summarized in Fig. 6. From Fig. 6(a), it was concluded that the yield of FA gradually decreased with the increase of the liquid flow rate. When FUR is not completely hydrogenated, a large amount of acetal (by-product) is generated with the increase of the liquid flow rate from 0.3 to 0.5 mL min^{-1}. The maximum yield of FA was 99.6% at 0.1 MPa and 0.1 mL min^{-1}. Also, the yield of FA could be improved when the pressure was 0.6 MPa, and the FA yield could reach 100% at a liquid flow rate of 0.6 mL min^{-1} as shown in Fig. 6(b). In Fig. 6(c), when ethyl acetate was used as the solvent, the yield of FA tended to increase and then decrease with the increase of the liquid flow rate. The maximum FA yield value of 99.9% was obtained at 0.6 mL min^{-1}. The main reason is the decreased residence time and elevated liquid hold-up caused by the increase of the liquid flow rate from 0.2 to 0.6 mL min^{-1}, which reduces the occurrence of the side reaction of hydrogenation of FA to 2-MF and enhances the external mass transfer. When the liquid flow rate is further increased from 0.6 to 1.0 mL min^{-1}, the influence of the mean residence time is significant, resulting in the insufficient hydrogenation of FUR in μPBRs. To achieve a rapid synthesis of FA, ethyl acetate is a more suitable solvent compared to isopropanol.

Table 3 Effect of the inlet FUR concentration

Inlet FUR concentration/mol L^{-1}	Solvent	X/%	Y_{FA}/%	$Y_{acetal\ by\text{-}product\ yield}$/%
0.2	Isopropanol	100	100	0
0.4	Isopropanol	100	98	2
0.6	Isopropanol	100	96	4
0.8	Isopropanol	67	42.2	24.8
1.0	Isopropanol	48	20.6	27.4
1.0	Isopropanol + 1 wt% H_2O	47	43	4
1.0	Isopropanol + 5 wt% H_2O	26	25.2	0.8
0.2	Ethyl acetate	100	99.9	0
0.4	Ethyl acetate	98	97.2	0
0.6	Ethyl acetate	52	52	0
0.8	Ethyl acetate	30	30	0
1.0	Ethyl acetate	20	20	0

Reaction conditions: 80 °C, 0.6 MPa, 0.6 mL min^{-1}, 20 sccm.

Effect of the initial FUR concentration

As shown in Table 3, with isopropanol as the solvent, the increase of the FUR concentration leads to the decrease of the FUR conversion and FA yield. The increase of the initial FUR concentration promoted the acetal reaction between alcohols and aldehydes. It is worth noting that the addition of water could effectively inhibit the formation of acetals at the expense of reducing the reaction rate.[11,42] When ethyl acetate was used as the solvent, the yield of FA decreased with the increase of the FUR concentration, but the selectivity to FA was not significantly affected. For the two types of solvents, it is evident that the increase of the initial concentration of FUR might result in more FUR adsorbed on the active sites and hinder the catalytic reaction.[40]

Catalytic transfer hydrogenation (CTH) of FUR in μPBRs

Gas molecular hydrogen is often used in catalytic hydrogenation reactions, which has the problem of higher costs and safety.[37] As a result, the catalytic transfer hydrogenation (CTH) process, as a typical liquid–solid reaction process, shows some advantages in conventional STRs compared to molecular hydrogen.[43] Here, the results for CTH of FUR to FA in μPBRs with Cu/SiO_2 are shown in Table 4. It can be seen from Table 4 (entries 1–3) that the yield of FA first increases and then decreases with the increase of temperature. On the one hand, the reaction rate accelerates with the increase of temperature ranging from 90 to 100 °C, thus promoting the formation of FA. On the other hand, the hydrogenolysis product 2-MF is formed with further increase of temperature ranging from 100 to 110 °C. The pressure was positively correlated with the FA yield, and the highest FA yield was 96.3% when the pressure was 3.1 MPa (entries 3–5). It can be noted that the addition of gas can significantly increase the yield of FA. This is because the perturbation of N_2 intensifies the liquid–solid mass transfer process and thus increases the reaction rate.[44] And when the gas flow rate was further increased, the effect of the gas flow rate on the FA yield was not significant (entries 2, 6 and 7). Meanwhile, the hydrogen donor isopropanol exhibited better performance compared to 2-butanol, which was consistent with the phenomenon observed by Zhu *et al.*[45] A possible reason for this phenomenon is that isopropanol has a lower viscosity (0.339 mPa s) compared to 2-butanol (0.680 mPa s) under the same conditions, resulting in a smaller mass transfer resistance.

Comparisons with different reactors

In order to compare the performance of different reactors, the space time yield (STY) was calculated by means of eqn (3):[23,24,46]

$$STY = \frac{m_{FA}}{V_R t} \quad (3)$$

where m_{FA} is the mass of the product FA, V_R is the volume of the reactor, and t is the reaction time. Also, t can be

Table 4 Catalytic transfer hydrogenation of FUR in μPBRs

Entry	T/°C	P/MPa	Solvent	N_2/sccm	Y_{FA}/%
1	90	0.6	Isopropanol	20	87.6
2	100	0.6	Isopropanol	20	94.3
3	110	0.6	Isopropanol	20	92.0
4	100	1.6	Isopropanol	20	95.6
5	100	3.1	Isopropanol	20	96.3
6	100	0.6	Isopropanol	0	21.0
7	100	0.6	Isopropanol	50	94.1
8	100	0.6	2-Butanol	20	68.5

Reaction conditions: 0.2 mol L^{-1} FUR, 0.2 mL min^{-1}.

Table 5 Comparison of the catalytic performance and STY for different reactors

	Reactor	Catalyst	Reaction time/h	T/°C	P/MPa	C_{FUR}/mol L^{-1}	Y_{FA}/%	STY/kg L^{-1} h^{-1}
H_2	STR[13]	Cu/SiO_2	4	110	1.0	0.2	21.4	0.000089
	STR[7]	$Cu/C–SO_3H$	2	105	0.4	0.2	99.9	0.0019
	PBR[49]	Pd–Cu/C	0.0633	180	2.1	0.47	31.1	0.033
	H-Cube mini reactor[21]	Ru/C	0.0094	90	5.0	0.2	82.4	0.59
	μPBR (this work)	Cu/SiO_2	0.018	80	0.6	0.4	98	0.51
CTH	STR[45]	ZrO_2	5	170	2	0.1	95.4	0.0018
	STR[50]	Fe/C	15	160	0.1	0.17	76.0	0.0002
	μPBR (this work)	Cu/SiO_2	0.054	100	0.6	0.2	94.3	0.08

considered as the mean residence time (τ), which can be obtained in the μPBR by eqn (4):[47]

$$\tau = \frac{\pi D^2 L \varepsilon h}{4Q} \quad (4)$$

where D is the inner diameter of the reactor, L is the length of the reactor, ε is the porosity of the μPBR and its value is 0.37, h is the liquid holdup, which can be determined from the literature,[48] and Q is the liquid flow rate.

Table 5 shows the catalytic performance and STY of FUR hydrogenation to FA in the conventional stirred tank reactor (STR), packed bed reactor (PBR), H-Cube mini reactor, and micropacked bed reactor (μPBR). Compared with the STR equipped with a Cu/SiO_2 catalyst, the μPBR was able to obtain high FA yields under mild conditions. Due to the excellent reactor properties of the μPBR, the FA yield can reach 99.6% with a short reaction time (65 s) at low temperature (80 °C) and low pressure (0.6 MPa) compared to the other reactors. Moreover, the maximum STY of the μPBR (0.51) is close to that of the H-Cube mini reactor (0.59), which is one to two orders of magnitude higher than those of the conventional STR and PBR. But the H-Cube mini reactor needs higher pressure (5 MPa) with respect to the μPBR (0.6 MPa). At the same time, the high cost of Ru-based catalysts used in the H-Cube mini reactor limits its industrial scale-up. For the CTH of FUR, the μPBR also provides an excellent STY at lower temperature and pressure as well as a larger STY in comparison to the conventional STR. In summary, both molecular hydrogenation and CTH of FUR can be performed efficiently and rapidly in μPBRs, and the performance of direct hydrogenation is superior to that of CTH of FUR.

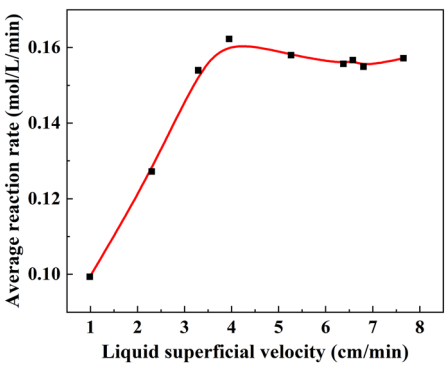

Fig. 7 Effect of different liquid superficial velocities on the reaction rate. Reaction conditions: 0.2 mol L^{-1}, 80 °C, 0.6 MPa, 20 sccm.

Kinetic investigation of FUR hydrogenation

The intrinsic kinetics for conversion of FUR to FA in μPBRs with molecular hydrogen is investigated. When isopropanol is used as the solvent, there is acetal by-product formation between FUR and isopropanol at low conversion, which may affect the accuracy of the kinetics data. Therefore, ethyl acetate was an appropriate solvent to evaluate the kinetic model for the hydrogenation of FUR to FA in μPBRs.

External diffusion. In gas–liquid–solid catalytic hydrogenation reactions, the external diffusion process entails two steps: hydrogen dissolved in furfural solution and furfural solution with hydrogen transferred to solid catalyst surface processes.[28,51] To investigate the intrinsic kinetics, the effect of external diffusion resistances should be ignored. The effect of external diffusion can be eliminated when the average reaction rate is not varied with the increase of liquid superficial velocities at the same liquid residence times. Therefore, μPBRs with the same volume (1.2 mL) and different inner diameters (3.87 mm, 4.35 mm, and 5.35 mm) were used to study the effect of different liquid superficial velocities on the reaction rate.

As shown in Fig. 7, the average reaction rate increased significantly when the liquid superficial velocity increased from 0.98 cm min^{-1} to 3.95 cm min^{-1}. This is mainly attributed to the larger liquid hold-up and effective gas–liquid interfacial area at the high liquid superficial velocity, which enhances the external mass transfer process.[26] When the liquid superficial velocity was further increased, the average reaction rate remained stable, indicating that the effect of external diffusion has been eliminated. Therefore,

Table 6 The value of each parameter for the M_W modulus

Parameter	Value	Unit
k'	0.02	m^3 liquid/(m^3 solid s)
L	100	μm
Porosity	0.37	—
Tortuosity	2.7	—
D_{eff}	9.50×10^{-10} for FUR 2.72×10^{-9} for H_2	m^2 s^{-1}
M_W	0.19 for FUR 0.006 for H_2	—

the liquid superficial velocity of 6.58 cm min^{-1} was chosen for the subsequent experiments.

Internal diffusion. Internal diffusion also affects the analysis of intrinsic kinetics due to pore limitations within the catalyst.[52] The Weisz modulus M_W (ratio of effective reaction time to diffusion time within the catalyst particle) of the substrate and hydrogen was calculated by eqn (5) and (6) to evaluate the limits of internal diffusion.

$$M_W = \frac{-k'L^2}{D_{eff}} \quad (5)$$

$$D_{eff} = \frac{\text{porosity}}{\text{tortuoxity}} D_m \quad (6)$$

where k' is the apparent reaction rate constant; L is the characteristic length of catalyst particles; D_{eff} is the effective diffusivity; D_m is the molecular diffusivity, which can be obtained in the literature.[52] The value of each parameter for the M_W modulus is calculated as shown in Table 6. The M_W of H_2 and FUR is less than 1, indicating that the effect of internal diffusion can be neglected.

Establishment of the kinetic model. A power-law model was employed to fit the relationship among the initial reaction rate (r), furfural concentration (C_A), and hydrogen pressure (P) as follows:

$$r = k'C_A^{\alpha}P^{\beta} = -\frac{dC_A}{dt} \quad (7)$$

where k' is the reaction rate constant, α is the reaction order of C_A, and β is the reaction order of P. Firstly, the residence time (τ) and hydrogen pressure were kept constant to determine the reaction order of C_A. In this regard, eqn (7) can be written as eqn (8). Considering the boundary conditions (t = 0, $C_A = C_{A0}$; $t = \tau$, $C_A = C_{A0}(1 - X/100)$), eqn (9) can be obtained as follows:

$$r = KC_A^{\alpha} = -\frac{dC_A}{dt} \quad (8)$$

$$X = \left(1 - \left[\frac{K\tau(\alpha-1)}{C_{A0}^{1-\alpha}} + 1\right]^{\frac{1}{1-\alpha}}\right) \times 100\% \quad (9)$$

Fig. 8(a) shows the relationship between the initial concentration and conversion of FUR. When C_{A0} increased from 0.08 mol L^{-1} to 0.29 mol L^{-1}, the conversion of FA decreased significantly. By fitting the data, α was 0.27. Then, the reaction order β can be obtained from eqn (10). And the reaction order for hydrogen pressure was 0.45 as shown in Fig. 8(b).

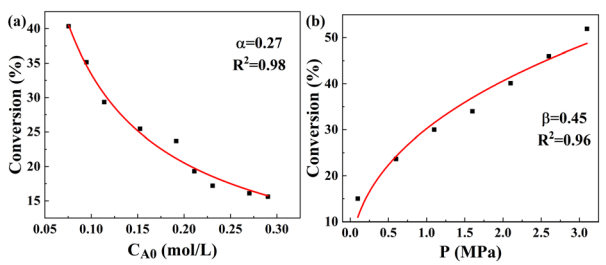

Fig. 8 Relationship between (a) the initial concentration of FUR and conversion and (b) hydrogen pressure and conversion. Reaction conditions: 80 °C, τ = 0.28 min, 20 sccm.

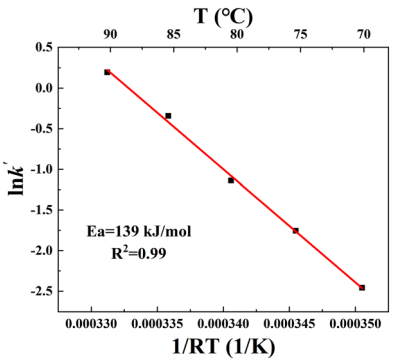

Fig. 9 Arrhenius plot of the reaction rate constants. Reaction conditions: 0.2 mol L^{-1}, 0.6 MPa, τ = 0.28 min, 20 sccm.

$$X = \left(1 - \left[\frac{k'P^{\beta}\tau(\alpha-1)}{C_{A0}^{1-\alpha}} + 1\right]^{\frac{1}{1-\alpha}}\right) \times 100\% \quad (10)$$

k' can be calculated by eqn (11) by using the values of α and β:

$$k' = \frac{C_{A0}^{0.73}\left[1-(1-X/100)^{0.73}\right]}{0.73P^{0.45}\tau} \quad (11)$$

The relationship between k' and temperature can be seen in Fig. 9. The intrinsic activation energy (E_a) of the FUR liquid-phase hydrogenation reaction to FA in μPBRs with the Cu/SiO_2 catalyst was 139 kJ mol^{-1} in the range of 70–90 °C, which was close to 127 kJ mol^{-1} for the CuMgAl catalyst[13] and 131 kJ mol^{-1} for the Cu/C–SO_3 catalyst, and less than 189 kJ mol^{-1} for the Cu/C catalyst.[37]

Concurrently, the Langmuir–Hinshelwood model was proposed to further understand the type of adsorption on the catalyst and the rate-controlling steps of the reaction. A range of Langmuir–Hinshelwood kinetic models have been reported for FUR hydrogenation to FA.[53–55] For these kinetic models, the model with non-competitive and dissociative adsorption of hydrogen and rate-controlling surface reaction provided the highest fitting degree (R^2 = 0.99).

$$r = \frac{kK_{FUR}C_{FUR}K_HP}{(1 + K_{FUR}C_{FUR} + K_{FA}C_{FA})(1 + \sqrt{K_HP})^2} \quad (12)$$

where k, K_{FUR}, K_H, and K_{FA} are the reaction rate constant and the adsorption equilibrium constants of FUR, H_2, and FA respectively.

Table 7 Values of various parameters for the Langmuir–Hinshelwood model

Parameter	k (mol g_{cata}^{-1} min^{-1})	K_{FUR}	K_{FA}	K_H
Value	1.31	27.39	1.95×10^{-16}	1.55

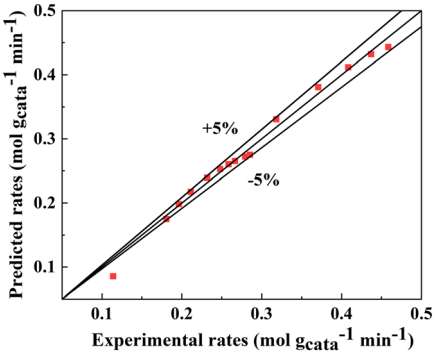

Fig. 10 Diagonal graph of the experimental and predicted rates (feed FUR concentration = 0.07–0.29 mol L^{-1}, hydrogen pressure = 0.1–3.1 MPa).

Table 7 shows the values of various parameters for the kinetic model at 80 °C. The reaction rate constant k for FUR hydrogenation to FA is 1.31 mol g_{cata}^{-1} min^{-1}. Comparisons for the predicted and experimental reaction rates can be seen in Fig. 10. The proposed correlation is considered reliable because the relative errors for values of the predicted and experimental rates are within ±5%. The obtained kinetic model helps to understand the rapid liquid-phase hydrogenation of FUR to FA in continuous μPBRs.

Conclusions

In this work, efficient and continuous hydrogenation of FUR to FA in μPBRs was studied. The performances of Cu-, Ni-, Pd-, and Pt-based catalysts for the furfural hydrogenation reaction were screened at different temperatures, and the Cu/SiO_2 catalyst was found to be more inclined to produce FA in μPBRs. Then the effects of solvent, pressure, gas and liquid flow rates, and initial concentration of FUR on the conversion of FUR and the yield of FA were discussed. FUR can be converted completely to FA under mild reaction conditions (80 °C and 0.6 MPa). For the catalytic transfer hydrogenation of FUR, μPBRs also provide the maximum yield of FA (96.3%) at 100 °C and 3.1 MPa. The space time yield of μPBRs is 0.51 kg L^{-1} h^{-1}, which is one to two orders of magnitude higher than those of conventional reactors. Moreover, the intrinsic reaction kinetics was investigated by neglecting the internal and external diffusion effects. The reaction rate is 0.27 order with respect to FUR and 0.45 order to hydrogen pressure. The intrinsic activation energy of the reaction is 139 kJ mol^{-1}. In addition, the experimental data were described by the Langmuir–Hinshelwood model. The model with non-competitive and dissociative adsorption of hydrogen and rate-controlling surface reaction provided the highest fitting degree. For furfural hydrogenation reactions, μPBRs provide a more efficient, fast, continuous, and safe molecular and catalytic transfer hydrogenation process.

Nomenclature

C_{FA}	Concentration of FA, mol L^{-1}
C_{FUR0}	Initial concentration of FUR, mol L^{-1}
C_{FUR}	Concentration of FUR, mol L^{-1}
D	Inner diameter of the micropacked bed reactor, m
D_{eff}	Hydrogen effective diffusion coefficient in the catalyst, m^2 s^{-1}
D_m	Hydrogen molecular diffusion coefficient, m^2 s^{-1}
E_a	Activation energy, kJ mol^{-1}
G	Gas flow rate, sccm
h	Liquid holdup of the micropacked bed reactor
k'	Reaction rate constant in eqn (7), $mol^{0.73}$ $L^{-0.73}$ $(MPa)^{-0.45}$ min^{-1}
k	Reaction rate constant in eqn (12), mol g_{cata}^{-1} min^{-1}
L	Characteristic length of catalyst particles, m
m_{FA}	Mass of furfuryl alcohol, kg
P	Hydrogen pressure, MPa
Q	Liquid flow rate, mL min^{-1}
T	Reaction temperature, °C
V_R	Reactor volume, L
X	Conversion of furfural
Y	Yield of furfuryl alcohol
τ	Liquid residence time, min
ε	Porosity of the reactor

Conflicts of interest

There are no conflicts to declare.

Acknowledgements

We gratefully acknowledge the support of the National Natural Science Foundation of China (21908126, 21978146, 22022809), the State Key Laboratory of Chemical Engineering (No. SKL-ChE-21A03), and the Beijing Institute of Technology Research Fund Program for Young Scholars in this work.

Notes and references

1 P. Sudarsanam, E. Peeters, E. V. Makshina, V. I. Parvulescu and B. F. Sels, *Chem. Soc. Rev.*, 2019, **48**(8), 2366–2421.
2 R. Mariscal, P. Maireles-Torres, M. Ojeda, I. Sádaba and M. López Granados, *Energy Environ. Sci.*, 2016, **9**(4), 1144–1189.
3 J. P. Lange, E. Van Der Heide, J. Van Buijtenen and R. Price, *ChemSusChem*, 2012, **5**(1), 150–166.
4 S. J. Canhaci, R. F. Perez, L. E. P. Borges and M. A. Fraga, *Appl. Catal., B*, 2017, **207**, 279–285.
5 X. Q. Wang, M. Qiu, R. L. Smith, J. R. Yang, F. Shen and X. H. Qi, *ACS Sustainable Chem. Eng.*, 2020, **8**(49), 18157–18166.
6 Z. D. An and J. Li, *Green Chem.*, 2022, **24**(5), 1780–1808.
7 W. B. Gong, C. Chen, H. M. Zhang, Y. Zhang, Y. X. Zhang, G. Z. Wang and H. J. Zhao, *Mol. Catal.*, 2017, **429**, 51–59.
8 J. Wu, G. Gao, J. L. Li, P. Sun, X. D. Long and F. W. Li, *Appl. Catal., B*, 2017, **203**, 227–236.

9 Q. Q. Yuan, D. M. Zhang, L. V. Haandel, F. Y. Ye, T. Xue, E. J. M. Hensen and Y. J. Guan, *J. Mol. Catal. A: Chem.*, 2015, **406**, 58–64.
10 K. E. Salnikova, V. G. Matveeva, Y. V. Larichev, A. V. Bykov, G. N. Demidenko, I. P. Shkileva and M. G. Sulman, *Catal. Today*, 2019, **329**, 142–148.
11 M. J. Taylor, L. J. Durndell, M. A. Isaacs, C. M. A. Parlett, K. Wilson, A. F. Lee and G. Kyriakou, *Appl. Catal., B*, 2016, **180**, 580–585.
12 C. Ramirez-Barria, M. Isaacs, K. Wilson, A. Guerrero-Ruiz and I. Rodríguez-Ramos, *Appl. Catal., A*, 2018, **563**, 177–184.
13 M. M. Villaverde, N. M. Bertero, T. F. Garetto and A. J. Marchi, *Catal. Today*, 2013, **213**, 87–92.
14 P. Jia, X. C. Lan, X. D. Li and T. F. Wang, *ACS Sustainable Chem. Eng.*, 2018, **6**(10), 13287–13295.
15 G. Singh, L. Singh, J. Gahtori, R. K. Gupta, C. Samanta, R. Bal and A. Bordoloi, *Mol. Catal.*, 2021, **500**, 111339.
16 R. López-Asensio, J. A. Cecilia, C. P. Jiménez-Gómez, C. García-Sancho, R. Moreno-Tost and P. Maireles-Torres, *Appl. Catal., A*, 2018, **556**, 1–9.
17 H. Yang, H. Chen, W. W. Lin, Z. Y. Zhang, M. W. Weng, W. H. Zhou, H. A. Fan and J. Fu, *Ind. Eng. Chem. Res.*, 2021, **60**(27), 9706–9715.
18 K. F. Jensen, *AIChE J.*, 2017, **63**(3), 858–869.
19 J. M. Bermudez, J. A. Menéndez, A. A. Romero, E. Serrano, J. Garcia-Martinez and R. Luque, *Green Chem.*, 2013, **15**(10), 2786–2792.
20 Y. T. Wang, P. Prinsen, K. S. Triantafyllidis, S. A. Karakoulia, A. Yepez, C. Len and R. Luque, *ChemCatChem*, 2018, **10**(16), 3459–3468.
21 A. J. Garcia-Olmo, A. Yepez, A. M. Balu, A. A. Romero, Y. Li and R. Luque, *Catal. Sci. Technol.*, 2016, **6**(13), 4705–4711.
22 A. Hommes, A. J. Ter Horst, M. Koeslag, H. J. Heeres and J. Yue, *Chem. Eng. J.*, 2020, **399**, 125750.
23 W. Y. Yang, X. J. Tang, W. J. Li, X. Luo, C. Y. Zhang and C. Shen, *Chem. Eng. J.*, 2022, **442**, 136110.
24 W. Z. Guo, T. Kortenbach, W. Qi, E. Hensen, H. Jan Heeres and J. Yue, *Appl. Catal., B*, 2022, **301**, 120800.
25 J. S. Zhang, A. R. Teixeira and K. F. Jensen, *AIChE J.*, 2018, **64**, 564–570.
26 L. Sang, X. D. Feng, J. C. Tu, B. Q. Xie, G. S. Luo and J. S. Zhang, *Chem. Eng. J.*, 2020, **393**, 124793.
27 X. N. Duan, X. P. Wang, X. K. Chen and J. S. Zhang, *Org. Process Res. Dev.*, 2021, **25**(9), 2100–2109.
28 J. C. Tu, L. Sang, H. Cheng, N. Ai and J. S. Zhang, *Org. Process Res. Dev.*, 2020, **24**(1), 59–66.
29 X. N. Duan, J. B. Yin, M. M. Huang, A. X. Feng, W. S. Fu, H. X. Chen, Z. F. Huang, Y. G. Ding and J. S. Zhang, *Chem. Eng. Sci.*, 2022, **248**, 117113.
30 X. N. Duan, J. C. Tu, A. R. Teixeira, L. Sang, K. F. Jensen and J. S. Zhang, *React. Chem. Eng.*, 2020, **5**(9), 1751–1758.
31 C. H. Zhang, X. N. Duan, J. B. Yin, F. Y. Lou and J. S. Zhang, *React. Chem. Eng.*, 2022, **7**, 1289–1296.
32 X. N. Duan, J. B. Yin, M. M. Huang, P. X. Wang and J. S. Zhang, *Chem. Eng. Sci.*, 2022, **251**, 117483.
33 G. Giorgianni, S. Abate, G. Centi, S. Perathoner, S. Van Beuzekom, S. H. Soo-Tang and J. C. Van der Waal, *ACS Sustainable Chem. Eng.*, 2018, **6**(12), 16235–16247.
34 Q. Q. Yuan, F. Y. Ye, T. Xue and Y. J. Guan, *Appl. Catal., A*, 2015, **507**, 26–33.
35 F. Dong, Y. L. Zhu, G. Q. Ding, J. L. Cui, X. Q. Li and Y. W. Li, *ChemSusChem*, 2015, **8**(9), 1534–1537.
36 W. Y. Ouyang, A. Yepez, A. A. Romero and R. Luque, *Catal. Today*, 2018, **308**, 32–37.
37 W. B. Gong, C. Chen, Y. Zhang, H. J. Zhou, H. M. Wang, H. M. Zhang, Y. X. Zhang, G. Z. Wang and H. J. Zhao, *ACS Sustainable Chem. Eng.*, 2017, **5**(3), 2172–2180.
38 N. S. Biradar, A. A. Hengne, S. N. Birajdar, R. Swami and C. V. Rode, Tailoring the product distribution with batch and continuous process options in catalytic hydrogenation of furfural, *Org. Process Res. Dev.*, 2014, **18**(11), 1434–1442.
39 Y. Nakagawa, K. Takada, M. Tamura and K. Tomishige, *ACS Catal.*, 2014, **4**(8), 2718–2726.
40 G. Chen, X. Zhu, R. Chen, Q. Liao, D. D. Ye, H. Feng, J. Liu and M. Liu, *Chem. Eng. J.*, 2018, **334**, 1897–1904.
41 X. N. Duan, J. B. Yin, A. X. Feng, M. M. Huang, W. S. Fu, W. F. Xu, Z. F. Huang and J. S. Zhang, *J. Flow Chem.*, 2022, **12**(1), 121–129.
42 N. Merat, C. Godawa and A. Gaset, *J. Chem. Technol. Biotechnol.*, 1990, **48**(2), 145–159.
43 M. J. Gilkey and B. J. Xu, *ACS Catal.*, 2016, **6**(3), 1420–1436.
44 S. P. Han, S. H. Li, H. B. Wang, W. Y. Yang, L. Sang and Z. P. Zhao, *Chem. Eng. Sci.*, 2022, **262**, 118033.
45 Z. K. Zhu, L. L. Yang, C. X. Ke, G. L. Fan, L. Yang and F. Li, *Dalton Trans.*, 2021, **50**(7), 2616–2626.
46 F. Liguori, P. Barbaro and N. Calisi, *ChemSusChem*, 2019, **12**, 2558.
47 Z. P. Peng, X. P. Wang, Z. Li, X. K. Chen, Y. J. Ding and J. S. Zhang, *React. Chem. Eng.*, 2022, **7**(8), 1827–1835.
48 J. S. Zhang, A. R. Teixeira, L. T. Kögl, L. Yang and K. F. Jensen, *AIChE J.*, 2017, **63**(10), 4694–4704.
49 M. Pirmoradi, R. J. Gulotty and J. R. Kastner, *Catal. Sci. Technol.*, 2020, **10**(20), 7002–7015.
50 J. Li, J. L. Liu, H. J. Zhou and Y. Fu, *ChemSusChem*, 2016, **9**(11), 1339–1347.
51 L. Duan, C. Ma, F. Y. Lou, J. B. Yin, L. Sang and J. S. Zhang, *Ind. Eng. Chem. Res.*, 2022, **61**(36), 13710–13719.
52 C. X. Yang, A. R. Teixeira, Y. X. Shi, S. C. Born, H. K. Lin, Y. L. Song, B. Martin, B. Schenkel, M. P. Lachegurabi and K. F. Jensen, *Green Chem.*, 2018, **20**(4), 886–893.
53 P. Liu, W. N. Qiu, C. Y. Zhang, Q. Q. Tan, C. Zhang, W. Zhang, Y. J. Song, H. Wang and C. Q. Li, *ChemCatChem*, 2019, **11**(14), 3296–3306.
54 P. D. Vaidya and V. V. Mahajani, *Ind. Eng. Chem. Res.*, 2003, **42**(17), 3881–3885.
55 S. Srivastava, G. C. Jadeja and J. Parikh, *Chem. Eng. Res. Des.*, 2018, **132**, 313–324.